Colloid Polym Sci (2009) 287:215–224
DOI 10.1007/s00396-008-1970-3

ORIGINAL CONTRIBUTION

Synthesis and characterization of new cholesteric monomers and smectic polymers containing menthyl groups

Jian-She Hu · Zhan-Xiang Zhao · Bo Kong · Dan Li

Received: 14 September 2008 / Revised: 15 November 2008 / Accepted: 17 November 2008 / Published online: 3 December 2008

Abstract New cholesteric monomers (M_2–M_5) and the corresponding smectic homopolymers (P_2–P_5) based on menthyl groups were synthesized. The chemical structures were characterized by Fourier transform infrared and ^{1}H NMR. The specific optical rotations were evaluated with a polarimeter. The structure–property relationships of the new compounds are discussed. The mesomorphism was investigated by differential scanning calorimetry, thermogravimetric analysis, polarizing optical microscopy, and X-ray diffraction. The selective reflection property of light was studied with UV/Visible/NIR. The monomers M_2–M_5 formed the cholesteric or blue phase when a flexible link chain was inserted between the mesogenic core and the terminal menthyl groups by reducing the steric effect. M_1 showed no mesomorphism, while M_2–M_5 revealed enantiotropic cholesteric phase. In addition, M_2 and M_3 also showed a cubic blue phase on cooling. The selective reflection of light for M_2–M_5 shifted to the short reciprocal wavelength region with increasing the temperature or intramolecular spacer length. P_2–P_5 exhibited the smectic A phase. The melting, clearing, and glass transition temperatures increased when increasing the aryl number in the mesogenic core or decreasing the intramolecular spacer length.

Keywords Menthyl groups · Liquid crystalline polymers · Cholesteric phase · Smectic A phase · Blue phase

J.-S. Hu (✉) · Z.-X. Zhao · B. Kong · D. Li
Center for Molecular Science and Engineering,
Northeastern University,
Shenyang 110004, People's Republic of China
e-mail: hujs@mail.neu.edu.cn

Introduction

Chiral liquid crystalline (LC) materials have attracted considerable interest because of their unique optical–electric properties, including the selective reflection of light, thermochromism, piezoelectricity and ferroelectricity, and potential applications such as nonlinear optical devices and full-color thermal imaging etc. [1–14]. Chirality can be introduced into LC molecules at various levels and is usually located in the terminal position of the mesogenic core. The rod-like, chiral molecules responsible for the macroscopical alignment of the mesogenic domains can form cholesteric, blue, or chiral smectic C phases. Depending on the chemical structure, it can achieve a macroscopic alignment of the chiral mesophase domains. In the recent year, many side-chain chiral LC polymers, mostly adopting commercially available chiral compounds, such as cholesterol [2, 4, 15, 16] and (*S*)-(+)-2-methyl-1-butanol [17–22], have been reported.

Menthol derivatives have been used as a chiral nonmesogenic monomer for the synthesis of side-chain LC copolymers [4, 23–32]. Bobrovsky et al. [25–28] reported detailed study on the LC copolymers by the polymerization of chiral nonmesogenic menthyl monomer and nematic or smectic monomer. Liu [31] also reported synthesis and characterization of novel monomers and polymers containing menthyl groups. Although these chiral monomers contained two or three phenyl rings, their mesogenic cores were directly linked to terminal menthyl groups, and the existence of the bulky steric menthyl groups prevented the formation of the LC phase, so they showed no any expected mesophase.

To date, to the best of our knowledge, the synthesis and characterization on the chiral mesogenic monomers and their corresponding LC homopolymers containing menthyl

groups have not been seen. We found that these monomers with three phenyl rings and their homopolymers containing menthyl groups could form cholesteric, blue, or smectic phases when a flexible link chain was inserted between the mesogenic core and the bulky terminal menthyl fragments by reducing the steric effect [33]. This is similar to the decouple effects observed when a flexible spacer is inserted between the polymeric main chain and the mesogenic side groups. Therefore, it is necessary to design and synthesize some novel chiral LC monomers and polymers derived from menthol to study their structure–property relationships and explore their potential applications. In this study, four new cholesteric monomers and their corresponding smectic homopolymers based on menthyl groups were prepared and characterized. Their mesomorphism and phase behavior were investigated with differential scanning calorimetry (DSC), thermogravimetric analysis (TGA), polarizing optical microscopy (POM), and X-ray diffraction (XRD). The selective reflection property of light was studied with UV/Visible/NIR. The structure–property relationships of these monomers and homopolymers are discussed.

Experimental

Materials

L-Menthol was purchased from Shanghai Kabo Chemical. Chloroacetic acid was purchased from Tianjin Bodi Chemical. 4-Hydroxybenzoic acid was obtained from Shanghai Wulian Chemical Plant. Allyl bromide and 2-chlorethyl alcohol were purchased from Beijing Chemical Reagent. 6-Chlorohexanol and 4, 4′-dihydroxybiphenyl (from Aldrich) were used as received. *N*, *N*′-Dicyclohexyl carbodiimide (DCC) was obtained from Shanghai Gongjia Chemical. 4-Dimethylaminopyridine (DMAP) was purchased from Jiangsu Wuxi Chemical. Polymethylhydrosiloxane (PMHS, $\overline{M}_n = 700 - 800$) was purchased from Jilin Chemical Industry. Toluene used in the hydrosilylation reaction was purified by treatment with $LiAlH_4$ and distilled before use. All other solvents and reagents used were purified by standard methods.

Measurements

Fourier transform infrared spectra were measured on a Perkin-Elmer spectrum One (B) spectrometer (Perkin-Elmer, Foster City, CA, USA). ^{1}H NMR spectra were obtained with a Bruker ARX400 spectrometer (Bruker, Swiss). The specific optical rotations were obtained on a Perkin-Elmer 341 polarimeter. The selective reflection wavelength was measured with a Perkin-Elmer 950 UV/Vis/NIR spectrometer with hot stage. The thermal properties were determined with a Netzsch DSC 204 (Netzsch, Germany) equipped with a cooling system. The heating and cooling rates were 10°C/min. The thermal stability of the polymers under nitrogen atmosphere was measured with a Netzsch TGA 209C thermogravimetric analyzer. The heating rates were 20°C/min. A Leica DMRX POM (Leica, Germany) equipped with a Linkam THMSE-600 (Linkam, England) hot stage was used to observe the phase transition temperatures and analyze the optical textures. XRD measurements were performed with a nickel-filtered Cu-K_α radiation with a DMAX-3A Rigaku (Rigaku, Japan) powder diffractometer.

Synthesis of the intermediate compounds

The synthetic route of the intermediate compounds is outlined in Scheme 1. Yields, melting temperatures, and IR characterization of the intermediate compounds **1–12** are summarized in Table 1. Menthyloxyacetic acid (**1**), 4-menthyloxyacetoxybenzoic acid (**3**), 4-allyloxybenzoic acid (**4**), 4-(2-hydroxyethoxy)benzoic acid (**5**), 4-(6-hydroxyhexyloxy)benzoic acid (**6**), and 4-(allyloxybenzoyloxy-2-ethoxy)benzoic acid (**7**) were prepared according to the method reported previously [33–36].

4-(Allyloxybenzoyloxy-6-hexyloxy)benzoic acid (8)

4-Allyloxybenzoyl chloride was prepared through the reaction of compound **4** with excess thionyl chloride according to the reported literature by Hu [36]. The acid chloride obtained (9.84 g, 50 mmol) was dissolved in 15 mL of tetrahydrofuran (THF) and then added dropwise to a solution of compound **6** (11.9 g, 50 mmol) in 200 mL of THF and 4 mL of *N*,*N*-dimethylformamide (DMF). The reaction mixture was refluxed for 30 h, cooled to room temperature, and then filtered. After the filtrate was concentrated by a rotary evaporator, the product was precipitated by adding ice-water to the filtrate, and recrystallized from ethanol; yield 62%, mp 139°C.

4-Hydroxylphenyl-4'-(allyloxybenzoyloxy-2-ethoxy) benzoate (9), 4-hydroxyl- phenyl-4'-(allyloxybenzoyloxy-6-hexyloxy)benzoate (10), 4-hydroxylbiphenyl-4'-(allyloxybenzoyloxy-2-ethoxy)benzoate (11), 4-hydroxylbiphenyl-4'- (allyloxybenzoyloxy-6-hexyloxy) benzoate (12)

The compounds **9**–**12** were synthesized by the same method. The synthesis of **10** is described below as an example.

4-(Allyloxybenzoyloxy-6-hexyloxy)benzoyl chloride was prepared through the reaction of compound **8** with excess thionyl chloride according to the similar method reported by Hu [36]. The acid chloride obtained (8.3 g, 20 mmol), dissolved in 20 mL of THF, was added dropwise

Scheme 1 Synthetic route of the intermediate compounds 1–12

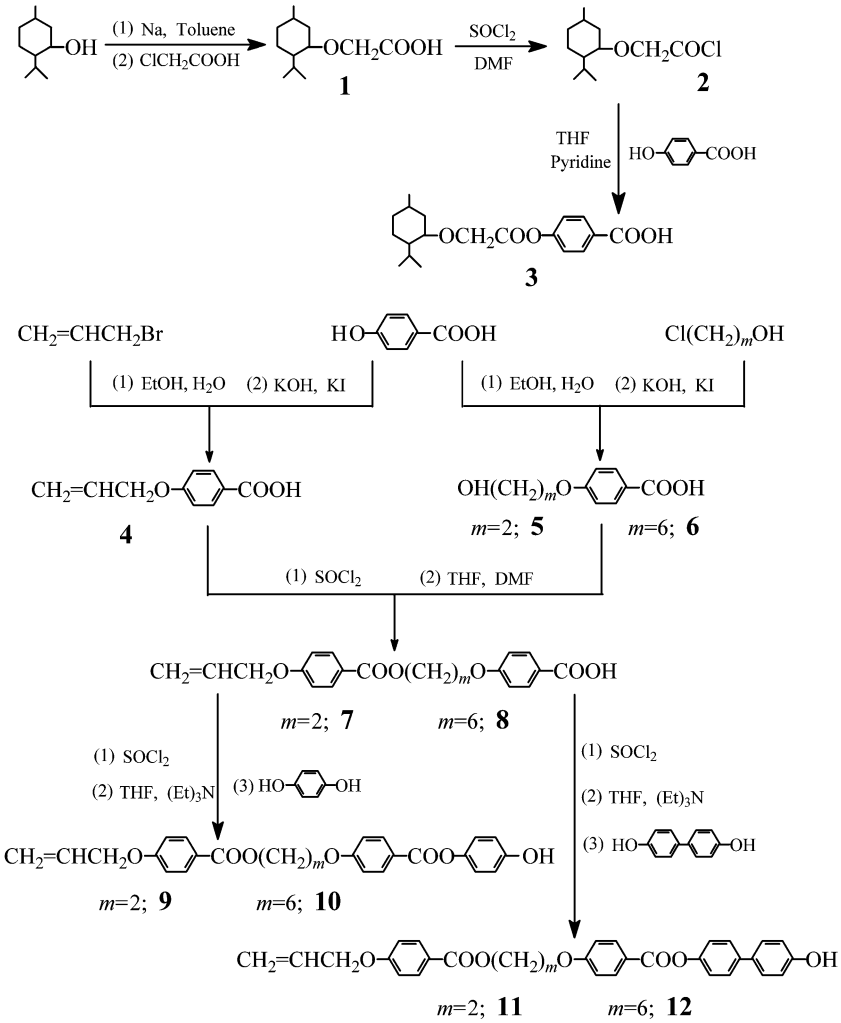

to a solution of *p*-benzenediol (11.0 g, 100 mmol) in 150 ml of THF and 3 mL of triethylamine under stirring. After the reaction mixture was refluxed for 24 h, the crude product was precipitated by adding water to the concentrated mixture and recrystallized from ethanol/acetone (3:1); yield 71%, mp 113°C.

Synthesis of the monomers

The synthetic route of the vinyl monomers is shown in Scheme 2. The chiral monomers M_1–M_5 were prepared by the same method. The synthesis of M_1 is described below as an example.

4-(Menthyloxyacetoxy)phenyl-4'-(allyloxybenzoyloxy-2-ethoxy)benzoate (M_1)

Compound **1** (2.58 g, 12.0 mmol) and compound **9** (4.35 g, 10.0 mmol) were dissolved in 100 mL of dry dichloromethane at 30°C. *N*,*N*′-Dicyclohexyl carbodiimide (DCC; 2.47 g, 12.0 mmol) and 4-dimethylaminopyridine (DMAP; 0.12 g, 1 mmol) were dissolved in 50 mL of dichloromethane and then added dropwise to the former solution. The reaction mixture was stirred for 30 h at 30 °C. The resulting solution was washed with 10 mL of water, stirred for 20 min, and filtered. After removing the water, the organic layer was dried with anhydrous magnesium sulfate, and concentrated by a rotary evaporator. The crude product was purified by column chromatography (silica gel, dichloromenthane), and recrystallized from ethanol/acetone (3:1). White solid was obtained; yield 54%, mp 66°C.

IR (KBr, cm^{-1}): 3,077 (=C–H); 2,956, 2,869 (–CH_3, –CH_2–); 1,778, 1,723 (C=O); 1,646 (C=C); 1,608, 1,513 (Ar–); 1,285 (C–O–C).

^{1}H NMR ($CDCl_3$, TMS, δ, ppm): 0.84–2.36 (m, 18H, menthyl–H); 3.32 (m, 1H, −CH< in menthyl); 4.41–4.66 (m, 8H, $-CH_2O-$ and $-COOCH_2-$); 5.34–5.51 (dd, 2H, CH_2=); 6.03–6.11 (m, 1H, =CH–); 7.01–8.20 (m, 12H, Ar–H).

Table 1 Yields, melting temperatures, and IR characterization of intermediate compounds

Compounds	Yield (%)	Recrystallized solvent	T_m (°C)	IR (KBr) (cm^{-1})
1	65	–	–[a]	3,645–2,565 (–COOH); 2,955, 2,871 (CH_3–, $-CH_2-$); 1,733 (C=O); 1,127 (C–O–C)
3	89	80% Ethanol	118	3,472–2,553 (–COOH); 2,959, 2,870 (CH_3–, $-CH_2-$); 1,783, 1,684 (C=O); 1,604, 1,506 (–Ar); 1,207, (C–O–C)
4	70	Ethanol	165	3,412–2,556 (–COOH); 1,693 (C=O); 1,644 (C=C); 1,605, 1,510 (–Ar); 1,251 (C–O–C)
5	64	Ethanol	181	3,308 (–OH); 3,265–2,552 (–COOH); 2,953, 2,865 ($-CH_2-$); 1,682 (C=O); 1,606, 1513 (Ar–); 1,253 (C–O–C)
6	55	Ethanol	132	3,404 (–OH); 3,243–2,531 (–COOH); 2,947, 2,869 ($-CH_2-$); 1,684 (C=O); 1,605, 1,513 (Ar–); 1,256 (C–O–C)
7	74	Ethyl acetate	151	3,364–2,556 (–COOH); 2,942, 2,825 ($-CH_2-$); 1,705, 1,679 (C=O); 1,606, 1,512 (Ar–); 1,252 (C–O–C)
8	62	Ethanol	139	3,300–2,554 (–COOH); 2,945, 2,859 ($-CH_2-$); 1,702, 1,679 (C=O); 1,607, 1,510 (Ar–); 1,253 (C–O–C)
9	72	Ethanol/acetone (2:1)	130	3,416 (–OH); 2,928, 2,863 ($-CH_2-$); 1,704 (C=O); 1,605, 1,509 (Ar–); 1,259 (C–O–C)
10	71	Ethanol/acetone (3:1)	113	3,428 (–OH); 2,940, 2,869 ($-CH_2-$); 1,706 (C=O); 1,606, 1,508 (Ar–); 1,260 (C–O–C)
11	48	Ethanol/acetone (1:1)	194	3,405 (–OH); 2,924 2,856 ($-CH_2-$); 1,730, 1,706 (C=O); 1,607, 1,511 (Ar–); 1,253 (C–O–C)
12	63	Acetone	175	3,400 (–OH); 2,937 2,860 ($-CH_2-$); 1,729, 1,706 (C=O); 1,607, 1,510 (Ar–); 1,256 (C–O–C)

[a] b.p. 162°C (1.34 kPa)

4-(Menthyloxyacetoxy)biphenyl-4'-(allyloxybenzoyloxy-2-ethoxy)benzoate (M_2)

Recrystallized from ethanol/acetone (1:1). White solid was obtained; yield 76%, mp 82°C.

IR (KBr, cm^{-1}): 3,071 (=C–H); 2,955, 2,869 ($-CH_3$, $-CH_2-$); 1,778, 1,731 (C=O); 1,646 (C=C); 1,605, 1,496 (Ar–); 1,259 (C–O–C).

^{1}H NMR ($CDCl_3$, TMS, δ, ppm): 0.83–2.37 (m, 18H, menthyl–H); 3.30 (m, 1H, −CH< in menthyl); 4.42–4.66 (m, 8H, $-CH_2O-$ and $-COOCH_2-$); 5.33–5.49 (dd, 2H, CH_2=); 6.04–6.10 (m, 1H, =CH–); 6.89–8.21 (m, 16H, Ar–H).

4-(Menthyloxyacetoxy)biphenyl-4'-(allyloxybenzoyloxy-6-hexyloxy)benzoate (M_3)

Recrystallized from ethanol/acetone (2:1). White solid was obtained; yield 61%, mp 71°C.

IR (KBr, cm^{-1}): 3,075 (=C–H); 2,953, 2,868 ($-CH_3$, $-CH_2-$); 1,774, 1,725 (C=O); 1,649 (C=C); 1,605, 1,499 (Ar–); 1,259 (C–O–C).

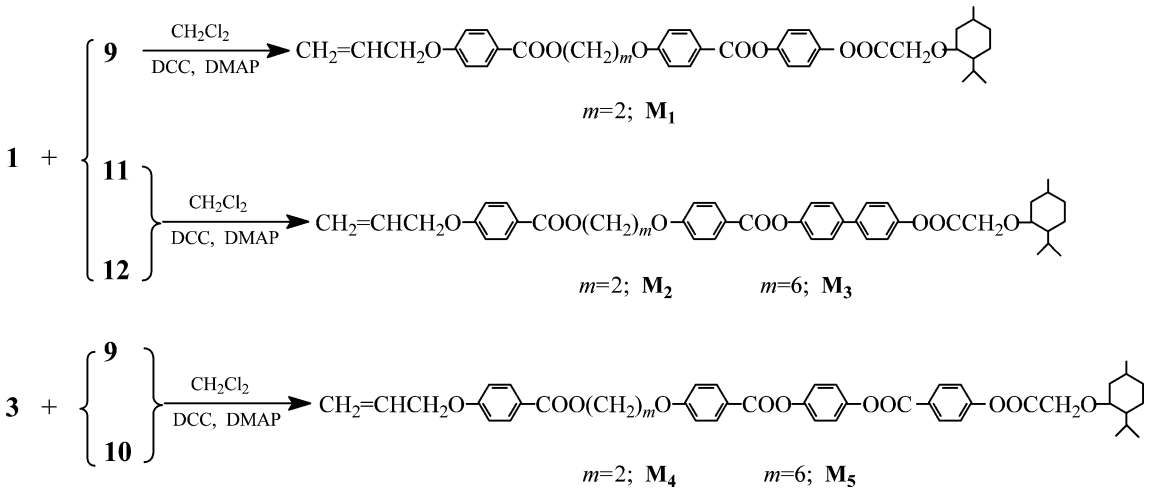

Scheme 2 Synthetic route of the monomers M_1–M_5

^{1}H NMR ($CDCl_3$, TMS, δ, ppm): 0.85–2.39 [m, 26H, menthyl–H and $-CH_2(CH_2)_4CH_2-$); 3.35 (m, 1H, −CH< in menthyl); 4.10 [t, 2H, $-(CH_2)_5CH_2O-$]; 4.43 [t, 4H, $-COOCH_2(CH_2)_5O-$ and $-OOCCH_2-$); 4.68 [t, 2H, $=CHCH_2O-$]; 5.35–5.52 (dd, 2H, $CH_2=$); 6.05–6.12 (m, 1H, =CH–); 7.00–8.22 (m, 16H, Ar–H).

4-(Menthyloxyacetoxybenzoyloxy)phenyl-4'-(allyloxybenzoyloxy-2-ethoxy)benzoate (M_4)

Recrystallized from ethanol/acetone (1:1). White solid was obtained; yield 52%, mp 97°C.

IR (KBr, cm^{-1}): 3,076 (=C–H); 2,955, 2,869 (–CH_3, –CH_2–); 1,780, 1,732 (C=O); 1,648 (C=C); 1,607, 1,510 (Ar–); 1,259 (C–O–C).

^{1}H NMR ($CDCl_3$, TMS, δ, ppm): 0.85–2.38 (m, 18H, menthyl–H); 3.33 (m, 1H, −CH< in menthyl); 4.44–4.67 (m, 8H, $-CH_2O-$ and $-COOCH_2-$); 5.35–5.53 (dd, 2H, $CH_2=$); 6.06–6.13 (m, 1H, =CH–); 7.01–8.26 (m, 16H, Ar–H).

4-(Menthyloxyacetoxybenzoyloxy)phenyl-4'-(allyloxybenzoyloxy-6-hexyloxy)benzoate (M_5)

Recrystallized from ethanol/acetone (2:1). White solid was obtained; yield 65%, mp 94°C.

IR (KBr, cm^{-1}): 3,076 (=C–H); 2,955, 2,869 (–CH_3, –CH_2–); 1,782, 1,733 (C=O); 1,649 (C=C); 1,606, 1,511 (Ar–); 1,263 (C–O–C).

^{1}H NMR ($CDCl_3$, TMS, δ, ppm): 0.84–2.39 [m, 26H, menthyl–H and $-CH_2(CH_2)_4CH_2-$); 3.34 (m, 1H, −CH< in menthyl); 4.15 [t, 2H, $-(CH_2)_5CH_2O-$]; 4.42 [t, 4H, $-COOCH_2(CH_2)_5O-$ and $-OOCCH_2-$); 4.67 [t, 2H, $=CHCH_2O-$]; 5.33–5.51 (dd, 2H, $CH_2=$); 6.07–6.15 (m, 1H, =CH–); 7.05–8.27 (m, 16H, Ar–H).

Synthesis of the homopolymers

The synthetic route of the homopolymers P_1-P_5 is shown in Scheme 3. They were prepared by the same method; the synthesis of P_1 is described as an example. M_1 (5 mol% excess versus the Si−H groups in PMHS) and PMHS were dissolved in dry freshly distilled toluene. The reaction mixture was heated to 65°C under nitrogen and anhydrous conditions, and then 2 ml of THF solution with the H_2PtCl_6 catalyst (5 mg/ml) was injected into the mixture with a syringe. The progress of the hydrosilylation reaction, monitored by the Si−H stretch intensity, went to completion, as indicated by IR. P_1 was obtained by precipitation from toluene solutions into methanol, purified by several filtrations from hot ethanol and then dried in vacuo.

Results and discussion

Synthesis

The synthetic routes of chiral monomers M_1-M_5 are shown in Scheme 2. Their structures were characterized by Fourier transform infrared (FT-IR) and ^{1}H NMR, which were consistent with the expected molecular design. IR spectra of M_1-M_5 showed characteristic stretching bands at about 1,782–1,774 cm^{-1} attributed to ester C=O in menthyloxyacetate and 1,733−1,723 cm^{-1} attributed to ester C=O in substituted benzoate. ^{1}H NMR spectra of M_1-M_5 showed multiplet at 6.15−5.33 ppm corresponding to olefinic protons in allyloxy groups. ^{1}H NMR spectrum of M_2 as an example is shown in Fig. 1.

The synthesis of polymers P_1-P_5 is outlined in Scheme 3. They were prepared through the hydrosilylation reaction

Scheme 3 Synthetic route of the homopolymers P_1-P_5

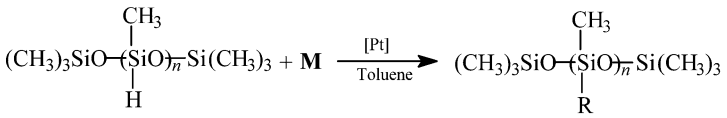

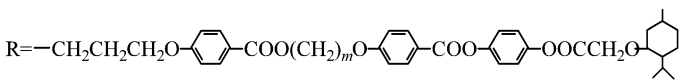

m=2; **P1**

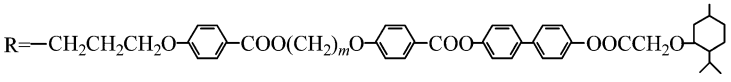

m=2; **P2** *m*=6; **P3**

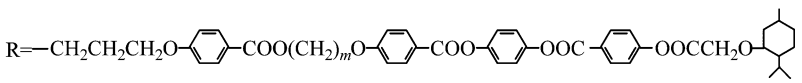

m=2; **P4** *m*=6; **P5**

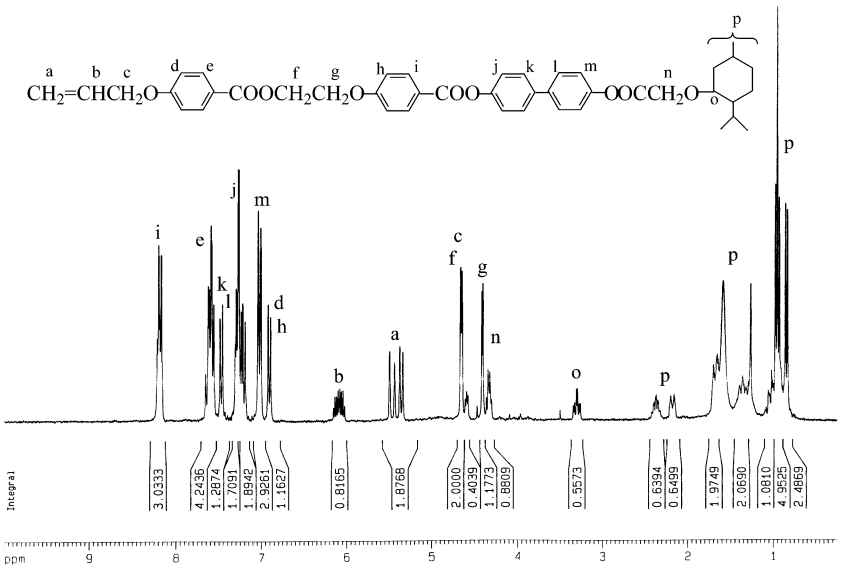

Fig. 1 ^{1}H NMR spectrum of M_2

using an excess amount of allyloxy monomers. The unreacted monomers were removed by several reprecipitations from toluene solutions into methanol and filtrations from hot ethanol. IR spectra of P_1–P_5 showed the complete disappearance of the Si–H stretching band at 2,165 cm^{-1} and olefinic C=C stretching band at 1,649–1,646 cm^{-1}. Characteristic Si–C bands appeared at about 1,257 and 783 cm^{-1}, and Si–O–Si bands appeared at about 1,166, 1,114, and 1,025 cm^{-1}. In addition, the absorption bands of methyl, methylene, ester C=O, and aryl still existed.

Specific optical rotations

The specific optical rotations of the monomers M_1–M_5 and the corresponding polymers P_1–P_5 were evaluated at 25°C in toluene. The results are listed in Tables 2 and 3. As can be seen from the data shown in Tables 2 and 3, the specific optical rotations of M_1–M_5 and P_1–P_5 were all left-handed, which indicates that the configuration or rotation direction of these new chiral compounds is hardly affected by a series of chemical reaction. According to Table 2, the specific optical rotation absolute values decreased when increasing the length of chiral molecules. Compared with M_1 $\left([\alpha]_D^{25} = -39.7^\circ\right)$, M_2 and M_4 with more aryl segments revealed lower specific optical rotation values. The results suggest that the existence of high conjugate biphenyl or more phenyl segments affects the molecular polarity. In addition, the monomers containing the same phenyl segment and the longer intramolecular spacer also showed the lower specific optical rotation values, for example, $[\alpha]_D^{25}$ of M_2 (m=2) was –31.0°, while that of M_3 (m=6) was –24.4°.

The specific optical rotation of P_1–P_5 showed the similar tendency as those described above for the corresponding monomers. Moreover, the specific optical rotation absolute values of P_1–P_5 were less than those of the corresponding monomers; this indicates that the concentration of optically active sites decreases because P_1–P_5 consist of optically inactive polysilioxane. This of course affects the amount of optically active sites, and this, in turn, decreases the optical rotation.

Table 2 Specific rotation, thermal properties, and mesophase of monomers

Monomer	m	$[\alpha]_D^{25}$ [a]	T_m/°C	ΔH_m/J·g^{-1}	T_i/°C	ΔH_i/J·g^{-1}	ΔT [b]	Mesophase
M_1	2	−39.7	66.2	70.3	–	–	–	–
M_2	2	−31.0	82.2	70.6	185.6	2.1	103.4	Ch
M_3	6	−24.4	71.8	39.2	177.1	1.2	105.3	Ch
M_4	2	−32.0	97.5	33.7	255.7	0.9	158.2	Ch
M_5	6	−23.0	94.5	32.0	241.7	1.7	147.2	Ch

Ch cholesteric
[a] 0.07 g in 25 mL of toluene
[b] Mesophase temperature range (T_i–T_m)

Table 3 Thermal properties and mesophase of polymers

Polymer	m	$[\alpha]_D^{25}$ [a]	T_g /°C	T_i [b] /°C	T_i [c] /°C	ΔT [d]	T_d [e] /°C	Mesophase
P_1	2	−32.2	17.3	–	–	–	315.6	–
P_2	2	−24.4	48.6	175.2	181.7	126.6	321.7	S_A
P_3	6	−19.6	29.0	166.4	174.1	137.4	318.5	S_A
P_4	2	−25.8	50.6	–	282.7	232.1	330.6	S_A
P_5	6	−18.3	38.2	–	273.5	235.3	327.2	S_A

[a] 0.06 g in 25 mL of toluene
[b] Temperature noted with DSC; S_A smectic A phase
[c] Temperature observed with POM
[d] Mesophase temperature range (T_i–T_g)
[e] Temperature at which 5% weight loss occurred

Thermal properties

The thermal properties of the monomers M_1−M_5 were investigated with DSC and POM. The phase transition temperatures, obtained on the second heating and cooling scans, corresponding enthalpy changes, and mesophase types of M_1−M_5 are summarized in Table 2.

DSC curves of M_1 showed only a single peak, and POM results also showed that M_1 exhibited no mesomorphism. However, DSC heating thermograms of M_2−M_5 all showed two endothermic peaks on heating and cooling cycles, which represent a melting transition and a cholesteric to isotropic phase transition, respectively. On cooling, two exothermic peaks were also seen, which represent an isotropic to cholesteric phase transition and a crystallization transition, respectively. All phase transitions are reversible, and the transition temperatures noted with DSC are consistent with those observed by POM.

The molecular structures had a considerable influence on the phase transition temperatures of M_1−M_5. Figure 2 showed the different phase temperature ranges of M_1−M_5. M_1 showed only a melting transition, and the LC to an isotropic phase transition did not appear because of the weaker rigidity of the mesogenic core. When increasing the rigidity of the mesogenic core or the number of aryl rings in monomer molecules, M_2−M_5 showed both the melting temperature (T_m) and the isotropic or clearing temperature (T_i). Compared with T_m of M_1, that of M_2 and M_4 increased by 16.0 and 31.3°C, respectively. In addition, a flexible intramolecular spacer also affected the phase transition temperatures. When a flexible intramolecular spacer m increased from 2 to 6, the corresponding T_m and T_i decreased. For example, compared with T_m and T_i of M_2 (m=2), those of M_3 (m=6) decreased by 10.4 and 8.5°C, respectively.

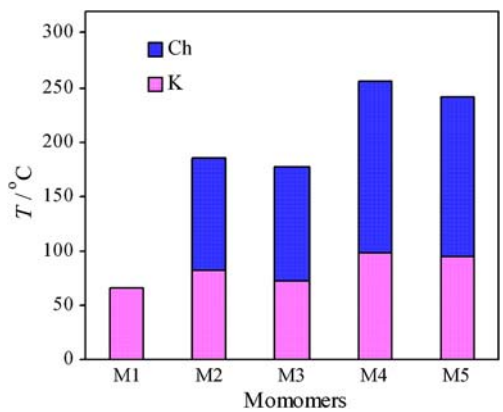

Fig. 2 Different phase temperature ranges of M_1−M_5

The thermal properties of homopolymers P_1−P_5 were studied with DSC, POM, and TGA. Their phase transition temperatures, thermal decomposition temperature, and mesophase types obtained are summarized in Table 3. DSC curves of P_1, P_4, and P_5 only showed the glass transition, but POM results indicated that P_4 and P_5 showed the mesomorphism, so T_i listed in Table 3 was according to the observation with POM. In addition, DSC thermograms of P_2 and P_3 showed both the glass transition temperature (T_g) and the LC to isotropic phase transition temperature.

In general, the thermal properties and mesomorphism of side-chain LC polymers mainly depend on the polymer backbone, the mesogenic core, the flexible intramolecular spacer, and the terminal groups [37]. T_g and T_i of LC polymers are very important parameters in connection with structures and properties. For P_1−P_5, because of the same polysiloxane backbone and terminal groups, the corresponding phase transition temperatures mainly depended on the nature of the mesogenic core and flexible intramolecular spacer. According to Table 3, the effect of mesogenic units and flexible intramolecular spacer on the T_g and T_i showed the similar tendency as those described above for the corresponding monomers. In addition, the mesophase temperature ranges of P_2−P_5 were greater than those of the corresponding monomers. This indicates that the polymerization can stabilize and widen the mesophases [15, 38].

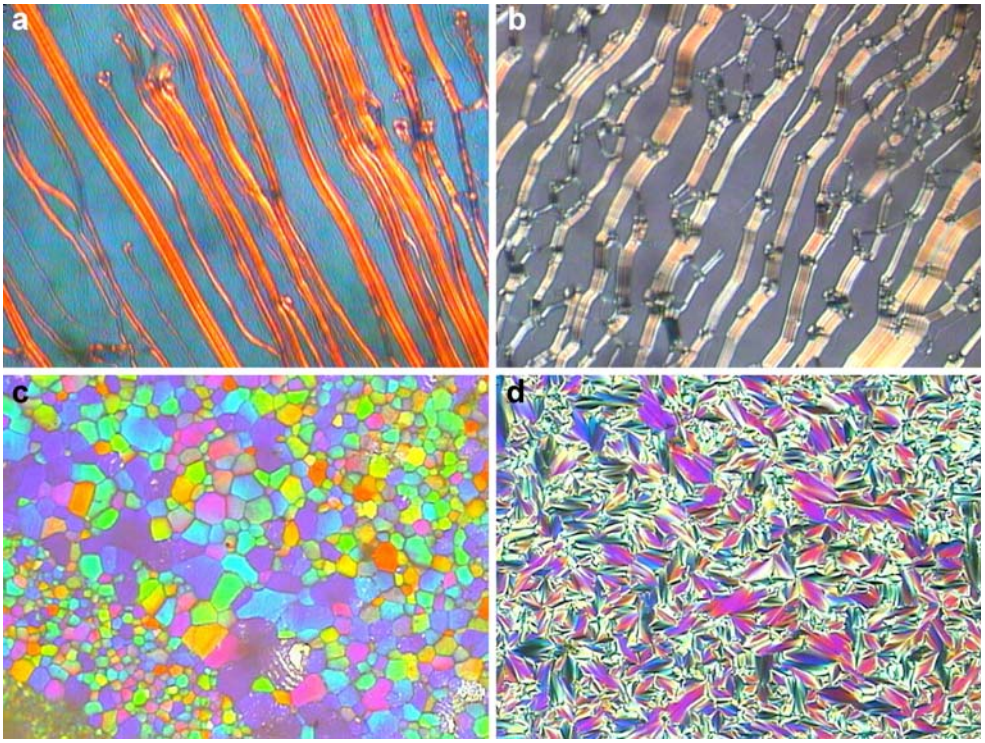

Fig. 3 Optical textures of monomers (200×). **a** Cholesteric oily streak texture on heating to 134.1°C for M_2; **b** cholesteric oily streak texture on heating to 171.6°C for M_3; **b** platelet texture of a cubic blue phase on cooling to 173.5°C for M_3; **d** cholesteric focal conic texture on cooling to 143.7°C for M_3

The thermal stabilities of P_1–P_5 were detected with TGA. The corresponding data are shown in Table 3. TGA results showed that the temperatures at which 5% weight loss occurred (T_d) were greater than 315°C for P_1–P_5; this indicates that all the homopolymers had good thermal stabilities.

Optical textures

In general, the cholesteric phase at zero field exhibits two optically contrasting stable states: planar (including oily streak and Grandjean) texture and focal conic texture. When cholesteric phase is in the planar state, the helical axis is perpendicular to the cell surface; when cholesteric phase is in the focal conic state, the helical axis is more or less parallel to the cell surface [38].

POM results showed that M_1 exhibited no mesomorphism, and M_2–M_5 all exhibited enantiotropic oily streak texture and focal conic texture of the cholesteric phase on heating and cooling cycles. In addition, M_2 and M_3 also exhibited platelet texture of a cubic blue phase (BP) on cooling from the isotropic melt. The BP exhibited different colors corresponding to different lattice planes, which shows Bragg scattering at different wavelengths, because the condition for constructive interference depends on the distance between lattice planes and their orientation with respect to the direction of incident light [39]. Further cooling, the platelet texture of cubic BP began to transform to the focal conic texture of the cholesteric phase. The typical optical textures of M_2 and M_3 are shown in Fig. 3a–d, respectively.

The homopolymer P_1 did not show mesomorphism, and P_2–P_5 exhibited the batonnet textures of the smectic A (S_A) phase, in this case, the smectic layers are basically perpendicular to the substrate plane. However, the cholesteric phase, exhibited for their corresponding monomers, did not appear. This indicates that the polymer chains hinder the formation of the helical supermolecular structure of the mesogens. It is also noted that the mesophase formed by side-chain LC polymers is more organized than that exhibited by the corresponding monomers. This behavior is attributed to an increased density of the mesogenic units in polymer side chain and, hence, an easier organization into the LC phases. Moreover, the LC polymers with siloxane macromolecular chains tend to form lower-order smectic phases. The optical texture of P_2, as an example, is shown in Fig. 4.

Selective reflection properties

The unique optical properties of cholesteric LC materials are related to their helical supermolecular structure. The periodic helical structure of cholesteric phase selectively reflects visible light like an ordinary diffraction grating, the pitch of which controls the wavelength of selective reflection of light. If the reflected wavelength lies in the visible range of the spectrum, the cholesteric phase exhibits brilliant colors. Due to the angular dependence of the

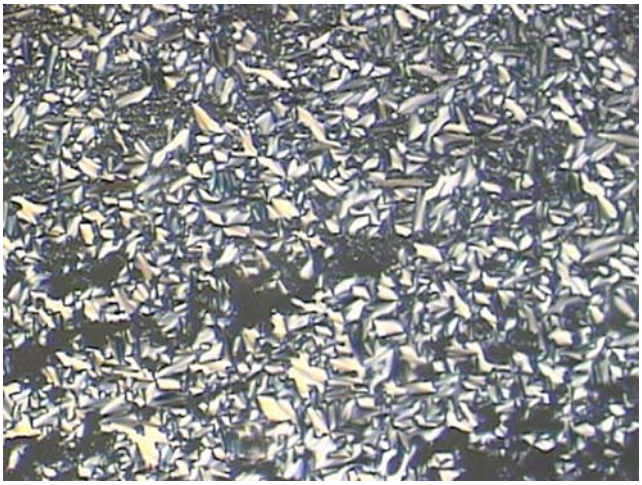

Fig. 4 Batonnet texture of a S_A phase at 143.5°C for P_2 (200×)

reflection conditions, the wavelength of the selective reflection of light λ obeys the Bragg condition [2].

$$\lambda = \overline{n}p\cos\theta \quad (1)$$

Where $\overline{n}$ is the average index of refraction, p is the pitch of the cholesteric phase, defined as the spatial distance over which the director rotates 360°, and θ is the incidence angle. When the normal incidence occurred, θ=0°, a maximum wavelength λ_m is described as follows:

$$\lambda_m = \overline{n}p \quad (2)$$

It is known that the pitch and the reflection wavelength depend on the molecular structure, such as the rigidity of mesogenic core, the nature of the terminal groups, and external condition (such as temperature, force, electric, and magnetic fields, etc). For M_2–M_5, the rigidity of mesogenic core not only affected the phase transition temperatures, but

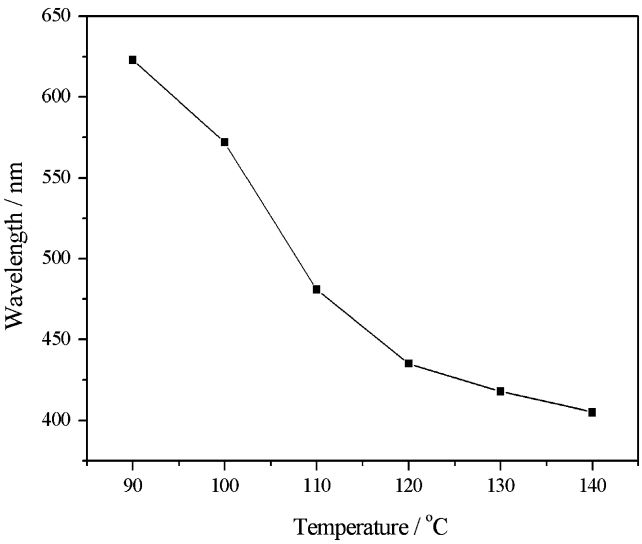

Fig. 5 Reflection wavelength as function of the temperature

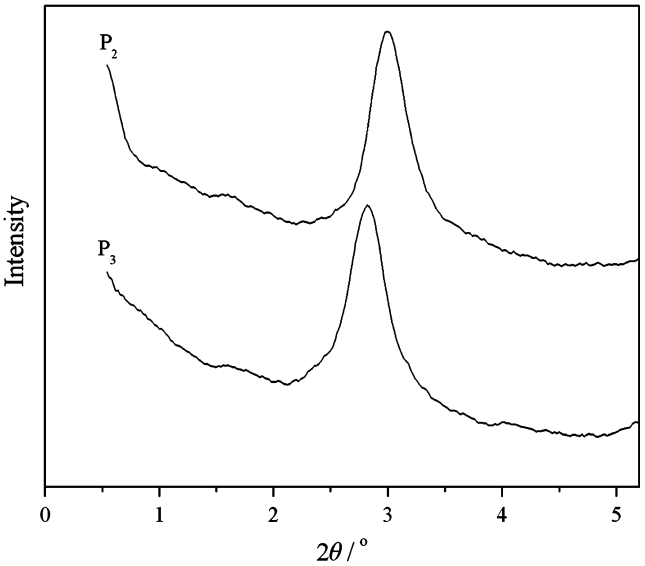

Fig. 6 XRD curves of P_2 and P_3

also the selective reflection colors. We found that the selective reflection color shifted to the short wavelength region (blue shift) when increasing the intramolecular spacer length in side chain. With increasing temperature, the reflection colors at the cholesteric phase exhibited pink, green, blue, and purple for M_2; green, blue, and purple for M_3; red, green, and blue for M_4; blue and purple for M_5. According to Eq. 1, an increase of the incidence angle made the selective reflection of light shift to the short wavelength region. To describe in detail the relationships of the maximum reflection wavelength λ_m and temperature, the λ_m of M_2, as an example, was measured by UV/Vis/NIR spectra with hot stage. Figure 5 shows the reflection wavelength as a function of the temperature. The λ_m decreased from 623 nm at 90°C to 405 nm at 140°C at the cholesteric phase. Therefore, the selective reflection wavelength showed a blue shift at the cholesteric phase with increasing temperature, so λ_m was temperature dependent.

XRD analysis

XRD studies were carried out to obtain more detailed mesophase type for LC materials. In general, a sharp peak associated with the smectic layers at small angle and a broad peak associated with the lateral packings at wide angle can be observed for smectic phase structure [17]. For P_2–P_5, XRD confirmed the presence of the S_A phase. Their X-ray patterns all exhibited a sharp reflection at small angle region associated with the smectic layers. Figure 6 shows the small angle XRD curves of P_2 and P_3 at mesophases. The *d*-spacing of the first-order reflections was 29.8 and 33.4 Å, respectively. Moreover, the *d*-spacing of the first-

order reflection hardly changed with temperature. This gives strong evidence for the formation of the S_A phase.

Conclusions

The synthesis of five new chiral monomers and their corresponding side-chain homopolymers, based on menthyl groups, is described and characterized. When increasing the length of chiral molecules, the monomers and homopolymers obtained showed lower specific optical rotation values. M_1 and P_1 showed no mesomorphism, while M_2–M_5 exhibited oily streak texture and focal conic texture of the cholesteric phase. Moreover, M_2 and M_3 revealed the platelet texture of a cubic BP on cooling. The selective reflection of light shifted to the short wavelength region when increasing the intramolecular spacer length for M_2–M_5. P_2–P_5 all exhibited the batonnet textures of the S_A phase. In addition, with increasing the aryl number in the mesogenic core or decreasing the intramolecular spacer length, the corresponding T_m or T_g and T_i increased. All of the obtained homopolymers displayed very good thermal stability.

Acknowledgement The authors are grateful to the National Natural Science Foundation of China, Program for New Century Excellent Talents (NCET) in the University, and Science and Technology Bureau of Shenyang for financial support of this work.

References

1. Broer DJ, Lub J, Mol GN (1995) Nature 378:467
2. Pfeuffer T, Strohriegl P (1999) Macromol Chem Phys 200:2480
3. Bacilieri A, Caruso U, Panunzi B, Roviello A, Sirigu A (2000) Polymer 41:6423
4. Lee YK, Onimura K, Tsutsumi H, Oishi T (2000) J Polym Sci Part A: Polym Chem 38:4315
5. Yeap GY, Nakata M, Takanishi Y, Ishikawa K, Takezoe H (2000) Liq Cryst 27:1437
6. Percec V, Obata M, Rudick JG, De BB, Glodde M (2002) J Polym Sci Part A: Polym Chem 40:3509
7. Shibaev PV, Kopp VI, Genack AZ (2003) J Phys Chem B 107:6961
8. Oaki Y, Imai H (2004) J Am Chem Soc 126:9271
9. Kaspar M, Bubnov A, Hamplova V, Novotna V, Lhotakova I, Havlicek J, Ilavsky M (2005) Mol Cryst Liq Cryst 428:49
10. Abraham S, Paul S, Narayan G, Prasad SK, Rao DSS (2005) Adv Funct Mater 15:1579
11. Brettar J, Burgi T, Donnio B, Guillon D, Klappert R, Scharf T, Deschenaux R (2006) Adv Funct Mater 16:260
12. Jeong SY, Ma YD (2007) Polym-Korea 31:356
13. Ohta R, Togashi F, Goto H (2007) Macromolecules 40:5228
14. Suda K, Akagi K (2008) J Polym Sci Part A: Polym Chem 46:3591
15. Hu JS, Zhang BY, Liu ZJ, Zang BL (2002) J Appl Polym Sci 86:2670
16. Hu JS, Zhang BY, He XZ, Cheng CS (2004) Liq Cryst 31:1357
17. Hsiue GH, Chen JH (1995) Macromolecules 28:4366
18. Hsu CS, Chu PH, Chang HL, Hsieh TH (1997) J Polym Sci Part A: Polym Chem 35:2793
19. Mihara T, Nomura K, Funaki K, Koide N (1997) Polym J 29:303
20. Merlo AA, Ritter OMS, Pereira FV, Vieira CH, da Silveira NP (2001) J Brazil Chem Soc 12:184
21. Soltysiak JT, Czuprynski K, Drzewinski W (2006) Polym Int 55:273
22. Zhang BY, Hu JS, Yang LQ, He XZ, Liu C (2007) Euro Polym J 43:2017
23. Mihara T, Nomura K, Funaki K (1997) Polym J 29:309
24. Altomare A, Andruzzi L, Ciardelli F, Gallot B, Solaro R (1998) Polym Int 47:419
25. Bobrovsky AY, Boiko NI, Shibaev VP (1998) Liq Cryst 24:489
26. Bobrovsky AY, Boiko NI, Shibaev VP, Wolff D, Springer J (1998) Macromolecules 31:5800
27. Bobrovsky AY, Boiko NI, Shibaev VP (1998) Ferroelectrics 212:387
28. Bobrovsky AY, Shibaev VP (2002) Adv Funct Mater 12:367
29. Hu JS, Zhang BY, Pan W, Zhou AJ (2005) Liq Cryst 32:441
30. Du BG, Hu JS, Zhang BY, Xiao LJ, Wei KQ (2006) J Appl Polym Sci 102:5559
31. Liu JH, Yang PC (2006) Polymer 47:4925
32. Liu JH, Yang PC, Hung HJ (2007) Liq Cryst 34:891
33. Hu JS, Wei KQ, Zhang BY, Yang LQ (2008) Liq Cryst 35:925
34. Lin HS, Deng YN (1998) Chin J Pharm 28:184
35. Hu JS, Zhang BY, Feng ZL, Wang HG, Zhou AJ (2001) J Appl Polym Sci 80:2335
36. Hu JS, Zhang BY, Zhou AJ, Yang LQ, Wang B (2006) Euro Polym J 42:2849
37. Le Barney P, Dubois JC, Friedrich C, Noel C (1986) Polym Bull 15:341
38. Ma RQ, Yang DK (1999) J Soc Inf Display 7:61
39. Dierking I (2003) Textures of liquid crystals. Wiley-Vch Verlag GmbH & Co. KGaA, Weinheim, pp 43–47